REPORT DOCUMENTATION PAGE

Form Approved
OMB No. 0704-0188

1. REPORT DATE *(DD-MM-YYYY)*	2. REPORT TYPE	3. DATES COVERED *(From - To)*
07-11-2007	Journal Article	

4. TITLE AND SUBTITLE

A Film Cooling Model for a RP-1/GOX Staged Combustion Liquid Rocket Engine (Preprint)

5a. CONTRACT NUMBER
F04611-00-C-0009

5b. GRANT NUMBER

5c. PROGRAM ELEMENT NUMBER

6. AUTHOR(S)
Philip A. Haberlen (Redstone Arsenol); Daniel A. Greisen (Sierra Engineering); William E. Anderson (Purdue University)

5d. PROJECT NUMBER

5e. TASK NUMBER
300500TU

5f. WORK UNIT NUMBER

7. PERFORMING ORGANIZATION NAME(S) AND ADDRESS(ES)

Sierra Engineering
603 East Robinson Street, Suite 7
Carson City, NV 89701-4046

8. PERFORMING ORGANIZATION REPORT NUMBER

AFRL-RZ-ED-JA-2007-489

9. SPONSORING / MONITORING AGENCY NAME(S) AND ADDRESS(ES)

Air Force Research Laboratory (AFMC)
AFRL/RZS
5 Pollux Drive
Edwards AFB CA 93524-7048

10. SPONSOR/MONITOR'S ACRONYM(S)

11. SPONSOR/MONITOR'S NUMBER(S)
AFRL-RZ-ED-JA-2007-489

12. DISTRIBUTION / AVAILABILITY STATEMENT

Approved for public release; distribution unlimited (PA #07457A).

13. SUPPLEMENTARY NOTES
For publication in the Journal of Propulsion and Power.

14. ABSTRACT

An experimental study of supercritical RP-1 film cooling was conducted in a RP-1/GOX rocket combustor. A heat sink test section, heavily instrumented with dual Type E coaxial thermocouples, was used for measurement of wall temperature and derived gas-side wall heat flux. Varying amounts of fuel, ranging from about 40% to 70% of the total fuel flowrate, were injected as a film coolant downstream of a coaxial injector element. An existing film cooling model was modified and applied to these experimental results. The resultant model predicted combustion chamber adiabatic wall temperature profiles for input propellant flow conditions and chamber geometry. The predicted wall temperatures were compared with the experimental measurements to assess the model's performance. The film cooling model wall temperature predictions had errors ranging from near 0 to ~33% compared to the experimental results for four out of five analyzed tests.

15. SUBJECT TERMS

16. SECURITY CLASSIFICATION OF:			17. LIMITATION OF ABSTRACT	18. NUMBER OF PAGES	19a. NAME OF RESPONSIBLE PERSON
					Dr. Richard Cohn
a. REPORT	b. ABSTRACT	c. THIS PAGE	SAR	31	19b. TELEPHONE NUMBER *(include area code)*
Unclassified	**Unclassified**	**Unclassified**			N/A

Standard Form 298 (Rev. 8-98)
Prescribed by ANSI Std. 239.18

A Film Cooling Model for a RP-1/GOX Staged Combustion Liquid Rocket Engine (PREPRINT)

Philip A. Haberlen[1]
Redstone Arsenal,AMSRD-AMR-PS-PT, Huntsville, AL 35898

Daniel A. Greisen[2]
Sierra Engineering Incorporated, Sacramento, CA, 95827

and
William E. Anderson[3]
Purdue University, West Lafayette, IN, 47907

An experimental study of supercritical RP-1 film cooling was conducted in a RP-1/GOX rocket combustor. A heat sink test section, heavily instrumented with dual Type E coaxial thermocouples, was used for measurement of wall temperature and derived gas-side wall heat flux. Varying amounts of fuel, ranging from about 40% to 70% of the total fuel flowrate, were injected as a film coolant downstream of a coaxial injector element. An existing film cooling model was modified and applied to these experimental results. The resultant model predicted combustion chamber adiabatic wall temperature profiles for input propellant flow conditions and chamber geometry. The predicted wall temperatures were compared with the experimental measurements to assess the model's performance. The film cooling model wall temperature predictions had errors ranging from near 0 to ~33% compared to the experimental results for four out of five analyzed tests.

I. Introduction

Liquid rocket engines (LRE) have energetic propellant combinations which are responsible for their high specific impulses. A result of this high energy release is high heat fluxes applied to the combustion chamber and nozzle walls. Many cooling mechanisms have been utilized to deal with these high heat fluxes, with fuel film cooling being used repeatedly for reusable, high performance LRE's. Fuel is typically used as the film coolant due to its thermochemical compatibility with the combustion chamber wall. To maximize the performance of a LRE the fuel film mass flow rate must be optimized. Optimization is required since too little film coolant flow results in inadequate wall cooling resulting in insufficient life or burn through; in contrast, too high film coolant flow results in an overcooled wall and an unacceptable decrease in engine performance.

[1] Aerospace Engineer, Redstone Arsenal, AMSRD-AMR-PS-PT, Bldg. 7120, Huntsville, AL 35898.
[2] Senior Staff Engineer, Sierra Engineering Incorporated, 3050 Fite Circle, #212, Sacramento, CA 95827.
[3] Associate Professor, School of Aeronautics and Astronautics, 315 N. Grant Street, West Lafayette, IN 47907.

Previous detailed studies on fuel film cooling have used simple configurations and either gaseous[1-9] or liquid[10-12] films to simulate the combustor flows. Gas film studies have emphasized the effects of reaction with the core flow, blowing and suction, and the effects of tangential injection. Gas film cooling effectiveness was defined based on dimensionless parameters. Liquid studies emphasized the measurement of liquid film length and entrainment. These studies have been done primarily under low-pressure, and whereas a few gas film studies considered the effects of reacting flows, most of the liquid film studies were limited to non-reacting conditions. A few studies have been undertaken in more practical systems,[13-18] albeit with limited measurement capability. Models for combustor film cooling are typically based on one-dimensional, fully-developed, laminar or turbulent flat-plate or pipe flow analogies. These models are severely limited by this lack of validation data under realistic conditions, and empirical correlations are often test-condition-specific. Finally, no experimental results are available which provide detailed measurements on the effects of hydrocarbon film cooling at supercritical pressure in a reacting flow situation.

Three objectives were established for the present program. The first objective was to review and assess current predictive models for fuel film cooling in rocket combustors, and to make necessary improvements to these models, emphasizing the operation at supercritical fuel film cooling conditions. The second objective was to evaluate measurement techniques for heat flux in rocket combustors, and to implement the best techniques in a test program. Finally, the third objective was to perform a series of hot fire tests, collecting experimental data on resultant wall conditions, and to compare these measurements to the predicted values over a range of operating conditions. Combination of these objectives results in a verified experimental/analytical approach capable of predicting the full-scale combustion chamber wall thermal environment. This tool could then be exercised to optimize the fuel film coolant flow rate during the design phase of a LRE.

This paper presents a literature review on past film cooling research and measurement techniques in Section IIA while Section IIB discusses the laboratory setup, test hardware, instrumentation, testing procedure, and data acquisition technique. Section IIC describes the film cooling model that was adapted to supercritical fuel film cooling, Section III contains test results and comparisons to model predictions, and Section IV summarizes this effort.

II. Approach

A. Literature Review

1. Film cooling research

Film cooling research conducted in the 1950's and 1960's can be roughly divided into gas and liquid film cooling experiments. Crocco[1] was one of the pioneering researchers in film cooling and investigated porous film cooling of a reactive coolant and showed theoretically that exothermic film coolants reduce film cooling effectiveness. Crocco hypothesized that liquid film coolant evaporates and diffuses from the boundary towards the combustion hot gas. The vapor is then confined in a laminar sublayer and behaves as a thermal barrier. This approach is widely adopted by the subsequent film cooling studies. Dorrance and Dore[2] investigated radial blowing and suction and its effects on the skin friction and heat transfer coefficients. Tangential film cooling injection has also been studied by many investigators.[3-9]. To determine the heat transfer coefficient for low thrust, low pressure rocket nozzle, Schoenman[49] separated the nozzle into turbulent and laminar regions. Before the laminarization point is reached, the one-dimensional turbulent Bartz equation is used, after which, laminar boundary layer theory is applied. Ewen and Evensen[50] accounted for changes in chamber contour, combustion gas properties and gas composition in their liquid film analysis. They used a one-dimensional pipe flow correlation to predict the convective heat transfer coefficient. Generally, these investigators correlated the film cooling effectiveness with various dimensionless groups including the mass flux ratio between the core gas and the film, the dimensionless distance downstream of the injection site, coolant Reynolds number, and others. For many studies, the final result was an empirically derived equation relating these quantities to the film cooling effectiveness.

Aside from the studies performed by Schoenman and Ewen and Evensen, most researchers adopted one-dimensional, fully-developed, turbulent flow over a flat-plate correlation to their liquid film cooling experimental results. Liquid film cooling investigations at low chamber pressure, below 150 psia, were conducted. Kinney, Abramson, and Sloop[10] conducted experiments with hot air traveling through 2- and 4-in diameter tubes that were liquid film cooled with water, water/detergent solutions, and aqueous ethylene glycol. Aside from the coolant types, hot core gas temperature, chamber pressure and coolant to hot gas mass flowrate ratios were varied to determine the corresponding liquid film-cooled length for different types of coolant injectors. They discovered a non-linear relationship between coolant flow rate and the liquid-cooled length. Their measured cooling effectiveness decreased with increasing coolant flow rate and a correlation was developed which predicted the minimum coolant flow rate. Kinney et al's model involved heavy empiricism and the units of the empirical constants in the correlation are disregarded. Knuth's doctoral dissertation[11] investigated liquid "film stability" and its effects on mass transfer due to

evaporation and unvaporized liquid droplet entrainment from the film surface to the core gas flow. Water, aqueous sucrose solution, aqueous zinc chloride solution, and carbon tetrachloride were used as coolants. Similarly, the varying test parameters included hot core gas temperature and chamber pressure. Gater and L'Ecuyer[12] extended these results further and discovered that mass transfer due to entrainment of unvaporized liquid droplets can exceed mass transfer due to evaporation from the film surface. The entrainment was postulated to shear off from the crest of the wave-like disturbances on the liquid film and is dependent on the roughness of the liquid film surface. A porous injector was employed with water, methanol, butanol, or hydrocarbon fuel, RP-1 in Gater's experimental investigations. Due to the designed experimental setup, the liquid coolant flowrate was deemed inaccurate and hence resulted in incorrect mass transfer observed.

Emmon[8] is one of the few experimental liquid film cooling investigation at relatively high chamber pressure (up to 780 psia). An empirical dimensionless heat transfer coefficient between hot core gas and liquid film was determined from an extensive test matrix. Test parameters include different hot core gas (hydrogen or air), hot core gas temperature, and chamber pressure. The effects of different coolants (water, aqueous ammonia solution, ethyl-alcohol, or Freon-113) on coolant requirements were also examined.

Fewer studies integrated the film cooling test results with a methodical analytical procedure for predicting the adiabatic wall temperature given known quantities in a LRE. Stechman[13] developed a model which predicted both liquid and gaseous film cooling effectiveness and applied it to two different LRE's which used monomethylhydrazine (MMH) as both the fuel and the film coolant. In addition to the film cooling effectiveness, a model was developed to determine the axial temperature distribution and liquid film-cooled length. In Stechman's approach, the heat transfer problem is broken into two parts: the heat transfer from the hot core gas to the film coolant, and the heat transfer from the film coolant to the wall. The turbulent heat transfer coefficient from hot core gas to film coolant is calculated using the modified Bartz equation and the heat transfer coefficient from the liquid film to the wall adopted the turbulent liquid film over a flat plate analysis. A stability correction factor was employed in the energy balance between the hot core gas and liquid film. The stability correction factor accounts for the liquid film stability, which depend strongly on the liquid film thickness. The predictions obtained from the model had errors ranging from about -20% to about 13% depending on the rocket engine analyzed and whether a fully turbulent or transition laminar flow model was used.

More recently, Grissom[14] conducted extensive review and discussion on the past liquid and gas film cooling experiments up to 1991 and derived a comprehensive model for film cooling under sub-critical conditions. In Grissom's comprehensive model, disturbances on liquid film surface, radiative heat transfer, freestream turbulence, foreign gas injection and turning effects on the flow due to chamber contour are all included. Yu[15] integrated Grissom's and Stechman's models for predicting the wall temperature of a sub-critical water cooled H_2O_2 rocket with mixed results. Following Yu's work, Haberlen[16] modified Grissom's model and applied the gaseous film cooling entrainment model of Rousar and Ewen[17-18] to a RP-1/GOX staged combustion LRE. This paper presents the liquid film cooling model of Reference 16.

2. Heat flux measuring techniques

Measurement of the heat flux on a combustion chamber wall in high-performance film cooled LRE is important because this demonstrates whether or not the film cooling provided adequate thermal protection. Several methods of measuring, or calculating, the gas-side wall heat flux have been developed. These include, but are not limited to, differential thermopile sensors, Gardon gauges, slug calorimeters, "null-point" calorimeters, coaxial thermocouples, "thin-film" sensors, and thermochromic liquid crystals. A reasonably comprehensive description of these techniques can be found in Reference 39. Coaxial thermocouples were chosen to measure wall temperatures, and derive the chamber wall heat fluxes for this study because they are durable, fast-responding, reasonably easily installed and removed, and because they present minimal interference to the gas flow inside the combustion chamber. Transient wall temperature measurements from a wind tunnel experiment has been successfully reduced to heat flux data;[47] in addition, finite difference techniques[33] and more efficient numerical algorithms that were specifically derived to convert surface temperature measurements into heat flux measurements have been described in the literature.[35-38] These studies formed the basis for the MATLAB computer program that was used to obtain the heat flux data from the coaxial thermocouples in this study. A detailed derivation of this computer program appears in Reference 16.

B. Experimental Setup

Tests were conducted on the 10,000 lb_f LRE test stand at the High Pressure Laboratory (HPL) in the Maurice Zucrow Laboratory Complex at Purdue University. Reference 16 describes the test set-up in detail. Figure 1 provides a schematic of the experimental hardware. The test set-up consists of two primary sub-assemblies; an oxygen rich preburner and an RP-1/GOX main combustion chamber. The preburner used hydrogen and liquid

oxygen to provide the hot oxygen-rich gas. Nominal preburner operating conditions are given in Table 1. The oxygen-rich gas generated in the preburner flowed through a sonic nozzle that fluidically isolated the preburner from the main chamber and a transition piece before it entered the oxidizer manifold of the main combustion chamber. A coaxial swirl fuel injector was used in the main combustion chamber.[19]

Fuel film cooling is injected parallel to the wall at two locations: the forward fuel film cooling ring (FFFC) and the aft fuel film cooling ring (AFFC). This paper presents only results from the barrel section between the FFFC and AFFC injection points, thus the following discussion is restricted to the FFFC, which is depicted in Fig. 2.

The forward film cooling injection ring applies RP-1 film coolant to the inside surface of the combustion chamber. The FFFC injection plane is located approximately 2.125 inch upstream of the instrumented test section. since the TCA igniter spool is located between the FFFC injector and the instrumented test section. Wall temperature measurements were made for the entire length of the combustion chamber and nozzle during the test program.

Table 1 Nominal Preburner Operating Conditions

Chamber pressure, (psia)	Gas temperature (°F)	Characteristic exhaust velocity (ft/sec)	Lox mass flow rate, (lb_m/sec)	GH_2 mass flow rate, (lb_m/sec)	Mixture Ratio (O/F)
1700	720	2055	3.45	0.022	157

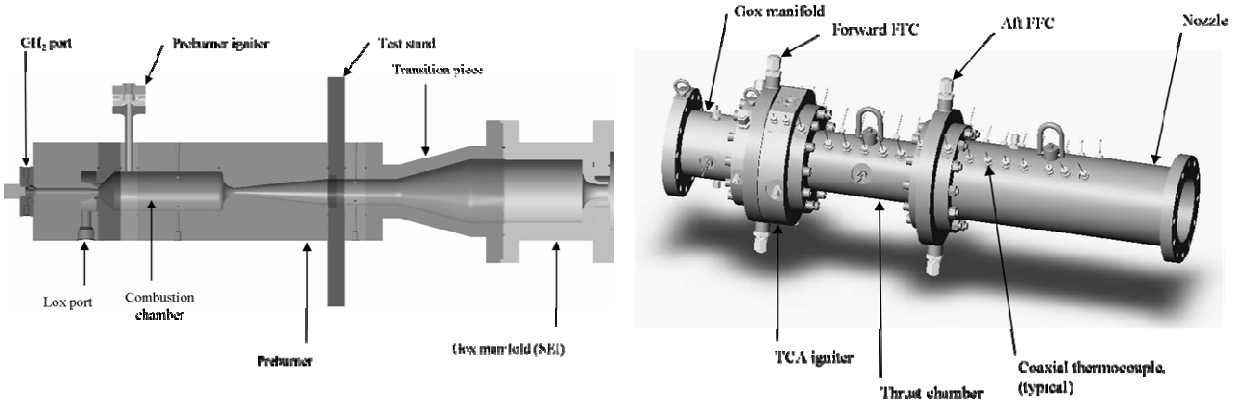

Figure 1 Schematic of Experimental Hardware.

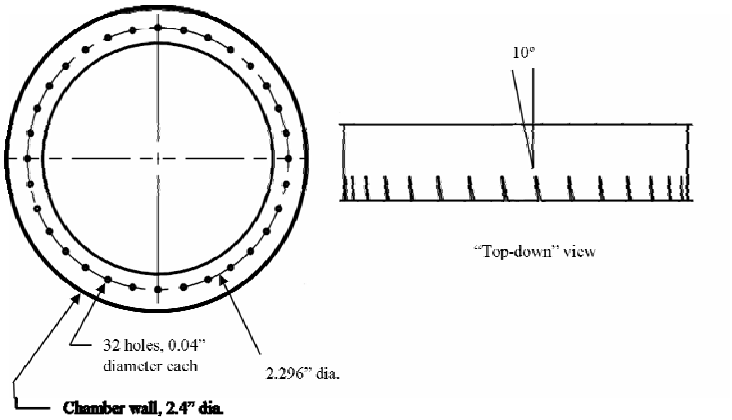

Figure 2 Forward Film Coolant Injection Ring Orifice Design (from SEI drawings).

The constant cross-sectional area of the combustion chamber was instrumented with Type E coaxial thermocouples. These coaxial thermocouples included the standard hot wall measurement and a recessed measurement located 0.2 inches behind the hot wall surface thermocouple. Two axial sets of coaxial thermocouples were installed in the combustion chamber. Figure 3 provides the axial and circumferential locations for the coaxial thermocouples. The axial sets of thermocouples were located on the 30^o (clockwise) and 60^o (counter clockwise) radial planes from vertical as shown in Figure 3. Each thermocouple is labeled as "TBAR1," "TBAR2," etc. as shown here and in the temperature plots of Sections IIIB through IIIF. These thermocouples were used to correlate the wall temperature predictions from the model.

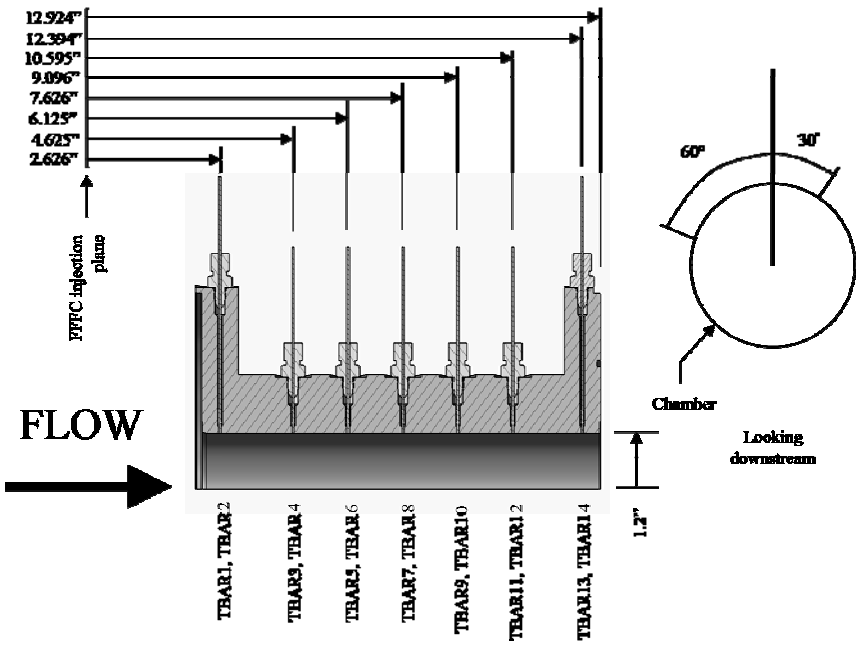

Figure 3 Coaxial thermocouple instrumentation planes for the main combustion chamber.

LabView 7.1 software was used for automatic control of the tests and data acquisition. All tests required two separate data acquisition systems due to the large array of instrumentation. The sampling rate was typically 500 Hz.

C. Film cooling analysis

1. RP-1 General description and properties

Supercritical RP-1 was used as the film coolant during the present test program. RP-1 is a mixture of many hydrocarbons, so it more properly has a critical pressure and temperature range. However, its critical pressure can be approximated as 315 psia and its critical temperature at 1215 ^{o}R. Thermophysical properties of RP-1 used during the current program were obtained from the Chemical Propulsion Information Agency's data on liquid propellants. RP-1 will undergo pyrolysis at high temperatures, which is colloquially known as "cracking." Various aspects of this phenomenon have been discussed in the literature, such as cracking kinetics, global mechanisms for the various cracking reactions, identifying the cracking products, investigating the coking and deposition properties of cracking, and modeling the "heat sink capacity" of cracking.[20-25] The "heat sink capacity" refers to the endotherm of the cracking process. The "endothermicity" of a fuel is relevant for film cooling since it enhances the film coolant's

ability to cool the walls relative to the non-cracking case. The details of how this was modeled are discussed in the next section.

2. Liquid film cooling model

Grissom's model[14] was modified to represent a supercritical liquid film coolant more appropriately. Figure 4 illustrates that the model slices the barrel axially into small sections (dx) and models the coolant temperature increase over each differential volume using conservation of energy. Central to this analysis is determining the energy transferred from combustion products to the coolant. This heat flux has both convective and radiative contributions. Each film coolant parcel (dx) absorbs the heat and experiences a temperature increase.

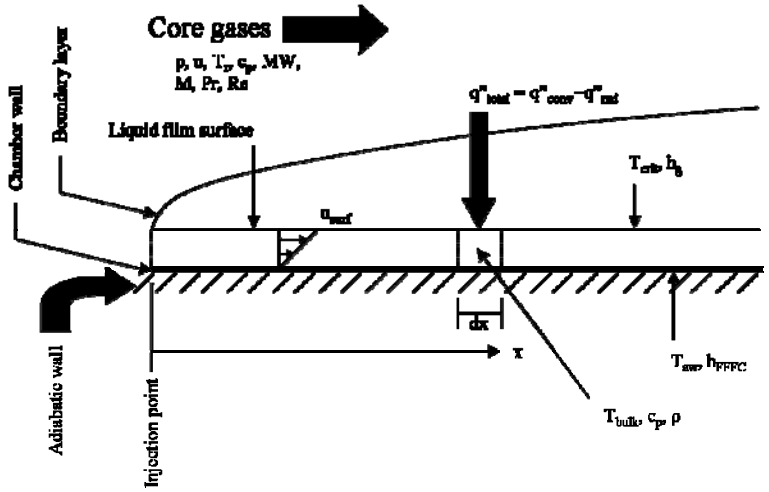

Figure 4 Liquid film cooling model schematic.

The following modeling assumptions were made:

1) The core gases are modeled as a steady, 1-D flow

2) There is 1-D heat transfer from the core gases in the radial direction only

3) RP-1/GOX reaction is "fast" compared to characteristic flow times – i.e. the combustion gases appear instantaneously at the upstream end of the barrel

4) The combustion gases do not react with the RP-1 film coolant

5) The film/wall interface is adiabatic and thus the surface thermocouples measure the adiabatic wall temperature

6) Viscous losses in boundary layer can be neglected due to the low Mach number in the barrel section

7) The velocity profile of the core gases in the boundary layer above the liquid film obey the turbulent 1/7 power law profile

8) The velocity profile in the liquid film is linear

9) The temperature gradient in the liquid film is negligible compared to the temperature gradient above the surface of the film

10) The surface of the liquid film (not the bulk temperature) is always at the RP-1 critical temperature

11) Negligible mixing occurs between the core gases and the liquid film

12) The liquid film thickness is constant from the injection point to its transition to a supercritical fluid

13) Knuth's correlation[11] accurately predicts the onset of large waves and significant unvaporized liquid entrainment into the core gas

14) The presence of species other than CO_2 and H_2O in the core gases can be ignored for radiation calculations

15) The thrust chamber barrel can be modeled as an infinite cylinder for radiation computations

16) The radiation heat flux from sooting is negligible compared to the core gas radiation heat flux

17) Inside wall absorptivity for irradiation was 0.5

To estimate the convective heat flux, q''_{conv}, the gas side heat transfer coefficient, h_g, was predicted. A flat plate correlation was used for this prediction:

$$St = \frac{1}{2} C_f \, \mathrm{Pr}^{-2/3} \tag{1}$$

where St is the Stanton number, C_f is the skin friction coefficient, and Pr is the Prandtl number of the core gases. The skin friction coefficient is computed from the Colburn Equation which assumes a 1/7 power law velocity profile inside the boundary layer:

$$C_f = 0.0592 \, \mathrm{Re}^{-0.2} \tag{2}$$

where Re_x is the Reynolds number of the core gases based on the distance from the leading edge of the plate. There is a large temperature difference between the core gases and the film surface, so it must be decided how to compute thermophysical properties since they are usually a strong function of temperature. Grissom's recommendation of evaluating the properties at the film temperature was followed.

Flat plate correlations predict high heat transfer coefficients near the leading edge and then predict much lower coefficients downstream. In fact, for x > 3.53D, where x is the distance from the injector and D is the chamber diameter, Eq. (1) predicts a lower heat flux than for fully-developed flow in a pipe. This is impossible since the heat flux predicted by fully-developed flow in a pipe must be the lower limit for heat transfer in a cylinder. Churchill and Usagi[26] determined that Eq. (2) can be used if the distance from the leading edge, x, is replaced by an "effective" distance, x_e:

$$x_e = 3.53D\left[1+\left(\frac{x}{3.53D}\right)^{-m}\right]^{-1/m} \tag{3}$$

where m is an empirical constant. Barbin and Jones[27] determined that m = 1.2 gives the best fit with their data based on Re_D = 388,000. The experiments in this paper had Re_D numbers very close to this value, thus, m = 1.2 was assumed.

To compute Re_x, the core gas mass flux is needed, evaluated at the mean temperature between the gas and the liquid film. It is computed as

$$G_{mean} = G_{chamber}\left(\frac{T_g}{T_{film}}\right)\left(\frac{u_g - u_l}{u_g}\right) \tag{4}$$

where $G_{chamber}$ is the core gas mass flux computed assuming no film cooling. The temperature ratio, (T_g/T_{film}), is the correction term for evaluating the gas density at the film temperature, where T_g is the core gas static temperature and T_{film} is the film temperature. The third factor is a correction for modeling the core gas flow relative to a moving film surface, where u_g is the core gas average velocity and u_l is the liquid film surface velocity.

Once G_{mean} is computed, h_g may be computed as $h_g = G_{mean}c_{pg}St$, where c_{pg} is the core gas specific heat evaluated at the film temperature and St is computed from Eq. (1) and (2). The heat capacity and Pr were computed assuming that the core gases consisted of equal mass fractions of CO_2, CO, and H_2O which cover most species expected to be present at the film temperature.

Free-stream turbulence can greatly enhance the heat transfer coefficient. Pletcher[28] asserts that the heat transfer coefficient is increased by a factor of $K_t = 1 + 4.0e_t$, where e_t is the root-mean-square turbulence fraction. Two

earlier studies[29-30] measured e_t in different types of LRE at various distances from the injector. These measurements indicated that e_t could range from 0.05 to 0.20. Due to the sparseness and scatter of these data, it was assumed that e_t = 0.10 for all the present tests.

Two possible types of liquid film disturbances might affect the convective heat transfer.[10-12] The two types are small, pebbled waves that are always present above a liquid film and large waves traveling in the flow direction. The large waves could result in significant mass loss due to liquid entrainment into the core flow. It was assumed that as long as Knuth's criteria were satisfied for the absence of large waves, no significant entrainment would occur. Knuth determined that if the mixture above the liquid film was mostly vapor and the vapor to liquid viscosity ratio is greater than 0.03, the critical liquid film mass flow rate per circumference is

$$\Gamma_{crit} = 101000 \frac{\mu_v^{\,2}}{\mu_l} \tag{5}$$

where μ_v and μ_l are the vapor and liquid viscosities, respectively. During this effort, the viscosity of the core gases was used for μ_v since no evaporation of the film coolant could take place. This condition was tested by the computer code and was satisfied in every test. It was assumed that the always-present small, pebbled waves would not affect h_g. Once these considerations are made, h_g can be computed and the convective heat flux is computed as $q''_{conv} = h_g(T_g - T_{crit})$, where T_g is the core gas static temperature and T_{crit} is the RP-1 critical temperature, which is assumed to be the surface temperature of the liquid film. Technically, the core gas static temperature should be replaced by the recovery temperature. However, since the Mach number in the barrel section is small (~ 0.14), this is a negligible distinction.

The core gas temperature was approximately 6700 ^oR for the present tests. Therefore, the radiation heat flux, q''_{rad} in Figure 4, could not be assumed negligible compared to the convective heat flux. Radiating gas species present in the core gas include H_2O, CO, CO_2, CH_4, and elemental carbon. Mass fractions were approximately 0.08, 0.52, 0.04, 0.08, and 0.25 respectively with other radical species constituting the remaining fraction. There are reliable data for the total emissivity of H_2O and CO_2 at 1 atm according to Siegel and Howell.[31] Grissom outlined a simple procedure for computing the total core gas emissivity for these two species.

The emissivity of each gas may be expressed as an empirical formula shown below:

$$\varepsilon = \varepsilon_f \left[1 + \left(\frac{\rho_{opt}}{c} \right)^{-n} \right]^{-1/n} \tag{6}$$

where ε_f is the "limiting value" emissivity at very high optical densities, ρ_{opt} is the optical density in atm*meters through the gas, and c and n are empirical constants that are functions of temperature. Table 2 lists these constants.

Table 2 Empirical constants for radiation model

H_2O			CO_2		
T, K	c (atm*m)	n	T, K	c (atm*m)	n
1000	0.165	0.45	1000	0.05	0.6
2000	0.90	0.65	1500	0.075	0.6
3000	2.05	0.61	2000	0.15	0.6

A polynomial fit was used to compute c and n for intermediate temperatures.

An additional correction term, K_p, is needed for pressures above 1 atm. Empirical expressions for these appear below:

$$\begin{aligned}
&H_2O : K_p = 1 + C_1 \left\{ 1 - \frac{\exp\left[\left(1 - P\left[1 + N_W \right] \right) \right]}{C_2} \right\} \\
&C_1 = 0.26 + 0.74 \exp\left(-2.5 \rho_{H_2O} \right) \\
&C_2 = 0.75 + 0.31 \exp\left(-10 \rho_{H_2O} \right) \\
&CO_2 : \log_{10} K_p = 0.036 \rho_{CO_2}^{\; -0.483\left[1 + (2 \log P)^{-m} \right]^{-1/m}} \\
&m = 100 \rho_{CO_2}
\end{aligned} \tag{7}$$

where P is the absolute pressure of the core gas in atmospheres, N_w is the mole fraction of H_2O, and ρ_{H2O} and ρ_{CO2} are the optical densities in [atmospheres*meters] for the appropriate species.

A correction factor, $\Delta\varepsilon$, is necessary to account for overlap between the two spectra for H_2O and CO_2. The method used to estimate this correction factor is presented below:

$$\begin{aligned}
&\Delta\varepsilon = 0.0551 K_n \left[1 - \exp\left(-4 \rho_{opt} \right) \right] \left[1 - \exp(-12.5 \rho_{opt} \right] \\
&K_n = 1 - \left| \frac{2 N_w}{N_w + N_c} - 1 \right|^n \\
&n = 5.5 \left[1 + \left(1.09 \rho_{opt} \right)^{-3.88} \right]^{-1/3.88}
\end{aligned} \tag{8}$$

where N_c is the mole fraction of CO_2 in the core gases. Following the calculation of $\Delta\varepsilon$ the total core gas emissivity was calculated as shown in Equation (9):

$$\varepsilon_g = \varepsilon_{H_2O} + \varepsilon_{CO_2} - \Delta\varepsilon \tag{9}$$

The optical path length through the core gases must be known to use Eqs. 8-9. The "overall effective length" may be used to approximate the optical path length. For an infinite cylinder, the overall effective length is L_{eff} = 0.95D, where D is the chamber diameter. Grissom justifies the infinite cylinder assumption by assuming that the cloud of droplets coming out of the main injector are perfectly reflective, an assumption that is used here.

Finally, Grissom considers the possibility of reflective chamber walls. Reflective walls increase the effective sight paths. Grissom cites a paper[32] asserting that the effective sight path can be multiplied by $A_w^{-0.85}$, where A_w is the wall absorptivity, assumed to be 0.5 for these tests. Once this final correction is made, the net radiant heat flux from the core gases to the liquid surface is expressed as:

$$q''_{rad} = \sigma A_w \varepsilon_g \left(T_g^{\,4} - T_{crit}^{\,4} \right) \tag{10}$$

where σ is the usual Stefan-Boltzmann constant and the other variables are the same as discussed previously.

Following the calculation of q''_{conv} and q''_{rad} one can derive an expression for the temperature rise of the film as it moves downstream. Applying conservation of energy to the differential control volume "dx" yields

$$q_{total} = q''_{total}\, \pi D(dx)(dt) = mc_p dT \tag{11}$$

where πD(dx) is the differential area on the surface of the control volume through which q''_{total} passes, dt is the time interval required for a fluid particle to travel the distance dx, m is the mass of coolant occupying the control volume at any instant in time, c_p is the specific heat, and dT is the differential temperature rise that the coolant experiences when passing through the control volume. It is known that dt = $dx/u_{average}$, where $u_{average}$ is the average velocity of the liquid film. Conservation of mass dictates that $u_{average} = m_{dot}/[\rho\pi D(thickness)]$, where m_{dot} is the mass flow rate of coolant, and πD(thickness) is the cross sectional area of the film. If one takes $\Gamma = m_{dot}/(\pi D)$ as the mass flow rate per circumference and substitutes this relationship and the earlier ones into Eq. 11, the following expression results after rearrangement:

$$dT_{bulk} = \frac{q''_{total}\,(dx)}{\Gamma c_p} \tag{12}$$

If the coolant/wall interface is adiabatic, then the bulk coolant temperature should be a reasonable approximation of the adiabatic wall temperature.

The possibility of endothermic pyrolytic reactions at high film temperatures was also considered. Huang, et al[25] studied the endothermic cracking properties of n-octane, JP-7, and JP-8. Their "endotherm" data for JP-8, see Figure 5, was used here because it more closely resembles RP-1 than the other two fuels studied.

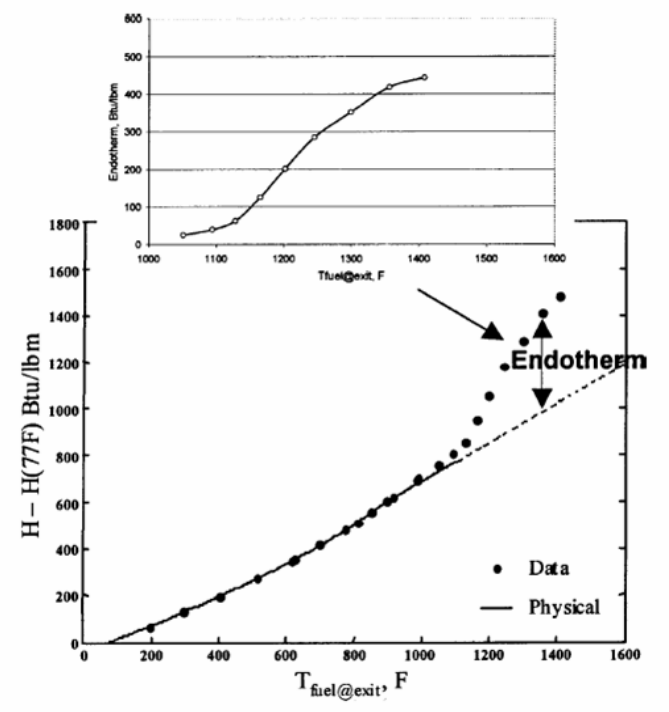

Figure 5 Endotherm data for JP-8, from Ref. [25].

The bottom graph compares real JP-8, represented by the dots, and a hypothetical JP-8 with its endothermic cracking reactions removed, represented by the dashed line. The upper graph plots the difference between the two. Significant endothermic effects do not appear until the temperature exceeds about 1050 °F. The slope of the dotted graph is the specific heat which includes the additional heat capacity of the endothermic cracking reactions. This specific heat is used in the film cooling model if the bulk film temperature exceeded 1050 °F.

A MATLAB computer program was written to predict the bulk film temperature as a function of axial distance, core gas conditions and film coolant injection flow rate. An abridged description of the program appears below. A more detailed step-by-step procedure appears in Reference 16.

1) Predict core gas conditions using Chemical Equilibrium and Applications CEA

2) Compute coolant thermophysical properties from reference data and test conditions

3) Compute core gas c_p and Pr at film temperature using property correlations

4) Compute G_{mean} from Eq. 4, x_e from Eq. 3, μ_{film} from property correlations, $Re_x = G_{mean}x_e/\mu_{film}$, C_f from Eq. 2, and St from Eq. 1

5) Compute gas side heat transfer coefficient, $h_g = K_t G_{mean} c_p St$ using $K_t = 1 + 4.0e_t$ using assumed $e_t = 0.10$, G_{mean} from 4), c_p from 3), and St from 4)

6) Test Knuth's criterion for presence of large waves and display warning if waves are present

7) Compute effective sight path, L_{eff}, optical density for H_2O and CO_2, and total gas emissivity based on the radiation model discussed earlier in this section

8) Compute total heat flux as $q''_{total} = h_g(T_g - T_{crit}) + \sigma\varepsilon_g A_w(T_g^4 - T_{crit}^4)$.

9) Compute bulk coolant temperature change and the new bulk temperature for the current axial location

10) If the coolant has reached critical temperature, begin using entrainment model;[16-18] if not, advance one axial step and return to step 1

11) Continue stepping down each axial location until the end of the barrel is reached

D. Error analysis

The relevant experimental measurements appear in the tables and figures of Sections IIIB through IIIF. They cover temperature, pressure, mass flow measurements, and calculated gas-side wall heat flux. Temperature and pressure were measured by thermocouples and pressure transducers. Mass flow rate was computed using a sonic venturi for the preburner GH_2 flow and a combination of turbine flowmeters and cavitating venturis for the preburner LOX flow and the RP-1 main injector and FFFC flows. Heat flux was obtained from the coaxial thermocouples via a 2-D transient finite difference technique.[33, 34] The details of the numerical derivation and computational procedure and comprehensive instrumentation lists may be found in Reference 16.

All coaxial thermocouples and the RP-1 main injector supply temperature measurement were Type E while the RP-1 FFFC supply temperature measurement was Type K. ANSI standards specify Type E accuracy as +/- 3.06 ^oR or 0.5%, whichever is greater and Type K standards as +/- 3.96 ^oR or 0.75%, whichever is greater. These uncertainties are valid for temperatures greater than 492^oR. The pressure transducers used for the TCA chamber

pressure measurements and the upstream cavitating venturi and sonic venturi computations had an uncertainty of +/- 12.5 psia.

The mass flow measurements for the liquid propellants, LOX and RP-1, were computed using a turbine flowmeter and a cavitating venturi. The turbine flowmeters for both the LOX and RP-1 lines had an uncertainty of 0.5% over the "linear range" of the meters. All the mass flows in this paper were within the linear range of the meters. Technically, turbine flowmeters measure volumetric flow rate, so the mass flow rate is obtained by simply multiplying by the liquid density. The liquid density uncertainty was assumed negligible compared to the flowmeter uncertainty.

Mass flow rates for the liquid propellants were also computed using cavitating venturi computations. The mass flow rate can be computed using Equation 13:

$$m_{dot} = C_d \frac{\pi}{4} d_2^{\,2} \left[\frac{2\rho g_c}{144} \left(P_1 - P_v \right) \right]^{1/2} \tag{13}$$

Where C_d is the discharge coefficient, d_2 is the venturi throat diameter in inches, ρ is the liquid density in lbm/ft^3, g_c is Newton's proportionality constant (32.174 lb_m-ft/(lb_f-s^2)), P_1 is the static pressure upstream of the venturi in psia, and P_v is the vapor pressure, also in psia. For a general function $R = R(x_1, x_2, \ldots x_n)$, the relative uncertainty in R due to random errors in $x_1, x_2, \ldots x_n$ can be expressed as

$$u_R = \pm \left[\left(\frac{x_1}{R} \frac{\partial R}{\partial x_1} u_1 \right)^2 + \left(\frac{x_2}{R} \frac{\partial R}{\partial x_2} u_2 \right)^2 + \ldots + \left(\frac{x_n}{R} \frac{\partial R}{\partial x_n} u_n \right)^2 \right]^{1/2} \tag{14}$$

where u_1, u_2, and u_n are the relative uncertainties for each of the independent variables that affect R. For all the tests in this paper, $m_{dot,\,Lox}$ = 3.45 lb_m/s, C_d = 0.993 +/- 0.01, d_2 = 0.124" +/- 0.001 in, ρ_{Lox} = 70.8 +/- 0.1 lb_m/ft^3, P_1 = 2615 +/- 12.5 psia, and P_v = 36.3 psia which was assumed to be known exactly. If Equation 14 is applied to Equation 13 for LOX with the previous conditions, then the mass flow rate uncertainty is 1.9%.

Similar calculations can be made for the cavitating venturis on the RP-1 main injector and FFFC injector. The main injector RP-1 conditions were constant for all tests. Assuming that $m_{dot,\,RP\text{-}1\ Main\ Injector}$ = 1.37 lb_m/s, C_d = 0.993 +/- 0.01, d_2 = 0.08 +/- 0.001 in, $\rho_{RP\text{-}1}$ = 50.8 +/- 0.1 lb_m/ft^3, P_1 = 3000 +/- 12.5 psia, and P_v = 0.16 psia (known exactly), this results in a mass flow rate uncertainty of 4.8%.

The mass flow rate, and thus its uncertainty, on the FFFC injector varied from test to test. The FFFC mass flow rates varied from 0.7 to 3.5 lb_m/s, $C_d = 0.993$ +/- 0.01, $d_2 = 0.06$ to 0.132 +/- 0.001 in depending on the desired flow rate, $\rho_{RP\text{-}1} = 50.8$ +/- 0.1 lb_m/ft^3, $P_1 = 3000$ +/- 12.5 psia, and $P_v = 0.16$ psia. With these conditions, the mass flow rate uncertainty varied from about 1.0% at 3.5 lbm/sec to 9.4% at 0.7 lbm/sec.

The mass flow rate for the preburner H_2 was measured using a sonic venturi and can be computed in the following way:

$$m_{dot} = C_d \frac{\pi}{4} {d_2}^2 P_1 \left[\frac{2 g_c \left(1+\frac{\gamma-1}{2}\right)^{\frac{-2\gamma}{\gamma^2-\gamma}} \left(\frac{\gamma}{\gamma-1}\right)\left(1-\left(1+\frac{\gamma-1}{2}\right)^{-1}\right)}{\left(1+B\frac{P_1 T_c}{T_1 P_c}\right) R T_1 \left(1-\left(\frac{d_2}{d_1}\right)^4 \left(1+\frac{\gamma-1}{2}\right)^{\frac{-2\gamma}{\gamma^2-\gamma}}\right)} \right]^{1/2} \qquad (15)$$

$$B = 0.083 - \frac{0.422}{T_r^{1.6}}$$

where γ is the specific heat ratio, T_1 is the upstream static temperature, T_c is the critical temperature, P_c is the critical pressure, R is the gas constant, d_1 is the inside wall diameter upstream of the venturi, and all other variables are as they were defined earlier in this section with the same units. For the conditions of these tests, $m_{dot,\ preburner\ GH2} = 0.022$ lb_m/s, $C_d = 0.9887$ +/- 0.01, $d_2 = 0.047$ +/- 0.001 in, $P_1 = 2125$ +/- 12.5 psia, $T_1 = 520$ +/- 3.96 ^oR, $d_1 = 0.18$ +/- 0.0053 in, R = 766.6 lb_f-ft/(lb_m-R), and $\gamma = 1.55$ for hydrogen at high pressure. Both R and γ are assumed to have negligible uncertainties. With these data, the uncertainty in the preburner H_2 mass flow rate is about 4.1%.

Finally, there is experimental uncertainty associated with the core gas mixture ratio (MR) computation. The core gas MR may be computed as

$$MR = \frac{m_{dot,Lox} - \frac{1}{2}\frac{MW_{O_2}}{MW_{H_2}} m_{dot,H_2}}{m_{dot,RP-1,maininjector}} \qquad (16)$$

It is assumed that the molecular weights have negligible uncertainties. The uncertainties in the LOX and RP-1 flows are higher for the cavitating venturi computations than for the turbine flowmeters, so those values were used to compute the uncertainty in MR to be conservative. The mass flow rate of GH_2 was computed using a sonic

venturi as discussed earlier. If the nominal mass flow rates for LOX, H_2, and RP-1 discussed previously are used as well as the computed relative uncertainties for these quantities, the uncertainty is 6.3% for MR.

The coaxial thermocouple heat flux uncertainty is presently unknown. Since the heat fluxes were obtained through an iterative numerical technique, no closed form expression exists which can be analyzed using Equation 14. A Monte Carlo simulation could be performed on the numerical model to estimate the uncertainty.

III. Results and Discussion

A. General remarks

Test results for six hot fire tests will be reviewed. Table 3 presents a summary of the hot fire test conditions for each test. The measured propellant conditions entering the combustion chamber and the main combustion chamber pressure are presented. As shown, the main injector flow conditions were maintained approximately constant, while the forward film cooling flowrate was varied from 0.880 to 3.617 lbm/sec. A faulty instrument precluded measurement of the "GOX" temperature entering the main injector, therefore, an estimate of this temperature was made using a MATLAB version of CEA. The estimated temperature of the "GOX", preburner exhaust gas, entering the main injector was 1160 ^{o}R.

Table 3 Summary of hot fire test conditions.

Test No.	RP-1 Main Inj. Temp.	Main Injector RP-1 Flowrate	Forward Film (RP-1) Temp	Forward Film (RP-1) Flowrate	Preburner H2 Flowrate	Preburner LOX Flowrate	MCC Pressure	Core MCC MR
	(^{o}R)	(lb_m/s)	(^{o}R)	(lb_m/s)	(lb_m/s)	(lb_m/s)	(psia)	
110905-171710	533	1.285	534	1.519	0.0255	3.519	808	2.6

110905-162107	536	1.314	531	1.844	0.0224	3.542	815	2.56
110905-131613	540	1.326	535	3.617	0.0222	3.607	818	2.59
112205-180505	514	1.316	520	1.643	0.0216	3.358	783	2.42
012606-192840	519	1.320	528	0.880	0.0214	3.489	770	2.51

Table 4 provides the predicted core gas parameters for each test. The parameters were estimated by CEA and are required for the film cooling analysis. Fore each test, the Pr and Re were about 0.48 and 380,000, respectively.

Table 4 Predicted core gas conditions.

Test No.	Recovery Temp	Core Density	Molecular Weight	Specific Heat	Γ	μ,	H_2O Mole Fraction	CO_2 Mole Fraction
	(^oR)	(lbm/in^3)	(lb_m/lb_{mole})	($Btu/lb_m/R$)		($lb_m/in\text{-}s$)		
110905-171710	6709	1.466e-4	23.0	1.703	1.137	6.359e-6	0.305	0.125
110905-162107	6701	1.472e-4	22.9	1.671	1.138	6.341e-6	0.307	0.133
110905-131613	6709	1.481e-4	23.0	1.69	1.137	6.355e-6	0.307	0.136
112205-180505	6639	1.396e-4	22.4	1.56	1.14	6.249e-6	0.304	0.120
012606-192840	6671	1.387e-4	22.7	1.65	1.14	6.305e-6	0.306	0.129

A figure is provided for each test which summarizes the model predictions as compared to "average" measured conditions during the steady state portion of the test.

The total gas emissivity that was computed as part of the radiation model described in Section IIC2 was 0.14 for all tests. Hydrocarbon/GOX mixtures can produce soot under the right conditions[48] and could conceivably contribute to the radiation heat flux. However, a simple analysis[16] indicated that under tested conditions radiant heat transfer from soot was negligible compared to the convective heat transfer.

Some of the thermocouples depicted in Figure 3, especially ones located near the injector, are not depicted in the figures that follow. These thermocouples gave obviously spurious results. Reference 16 provides the raw temperature plots and further details on which thermocouple data were discarded.

B. 11905 171710 test results

Figure 6 presents the measured, average hot wall temperature as compared to the predicted hot wall temperature. The difference between prediction and measurement ranged from about -5% to about 30%. When predicting h_g using a flat plate correlation, the heat transfer coefficient is very high near the injector and decreases rapidly, resulting in predicted heat fluxes near the injector which are higher than those extracted from the measured data. This partly explains why the predicted film temperature rises quickly near the injector and then rises more slowly further downstream. This shape is a feature of most of the tests.

Complete graphs of derived heat fluxes from each coaxial thermocouple for each test appear in Reference 16. Predicted heat fluxes for this test range from 0.5 near the injector to 2.0 Btu/in^2-s further downstream. Compared to the total heat flux predicted by the film cooling model, these heat fluxes are almost negligible in the upstream portion of the barrel but become approximately 30-40% of the applied heat flux in the downstream portion. Thus, the adiabatic wall assumption becomes progressively worse as one moves downstream for the identified modeling assumptions.

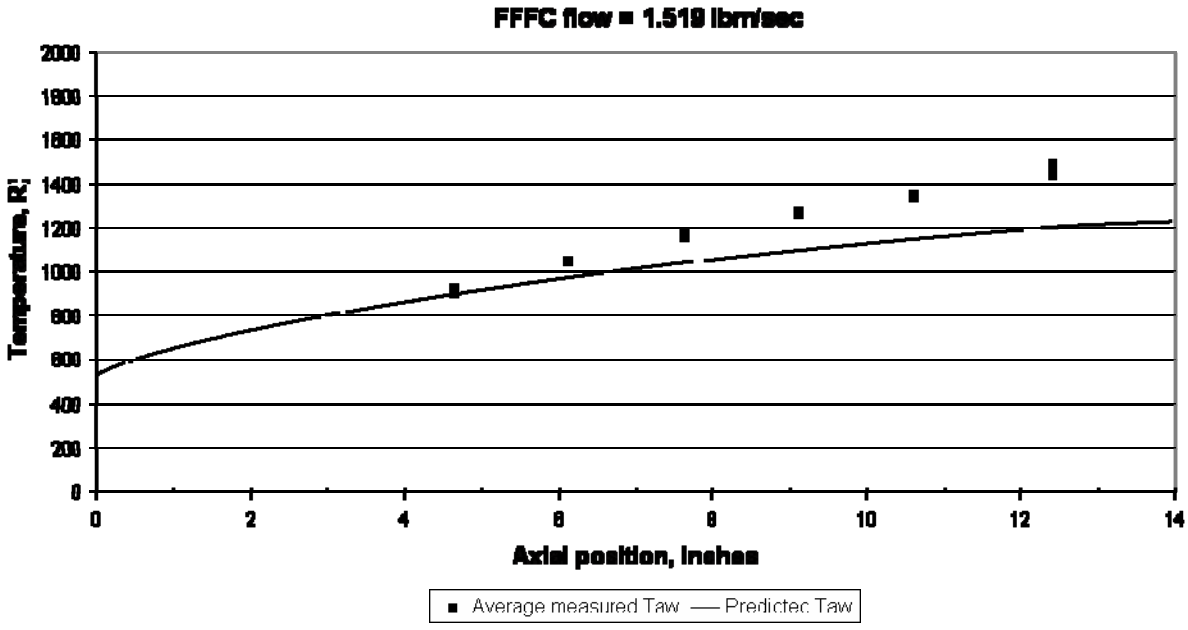

Figure 6 Predicted and averaged experimental results for 110905-171710.

C. 11905 162107 test results

Figure 7 presents the measured, average hot wall temperature as compared to the predicted hot wall temperature for test 11905-162107.The shape of the predicted wall temperature curve is similar to the previous test except that the predicted and experimental temperatures are lower due to the increased film cooling mass flow rate. The error between the predicted and experimental wall temperatures ranged from about -16% near the end of the barrel to near zero further upstream.

The heat flux ranges from 0 – 1.5 Btu/in^2-s, which are slightly lower than the earlier test. This helps strengthen the adiabatic wall assumption especially near the downstream end of the barrel, although the heat flux through the walls still constituted about 30% of the applied heat flux near the downstream end.

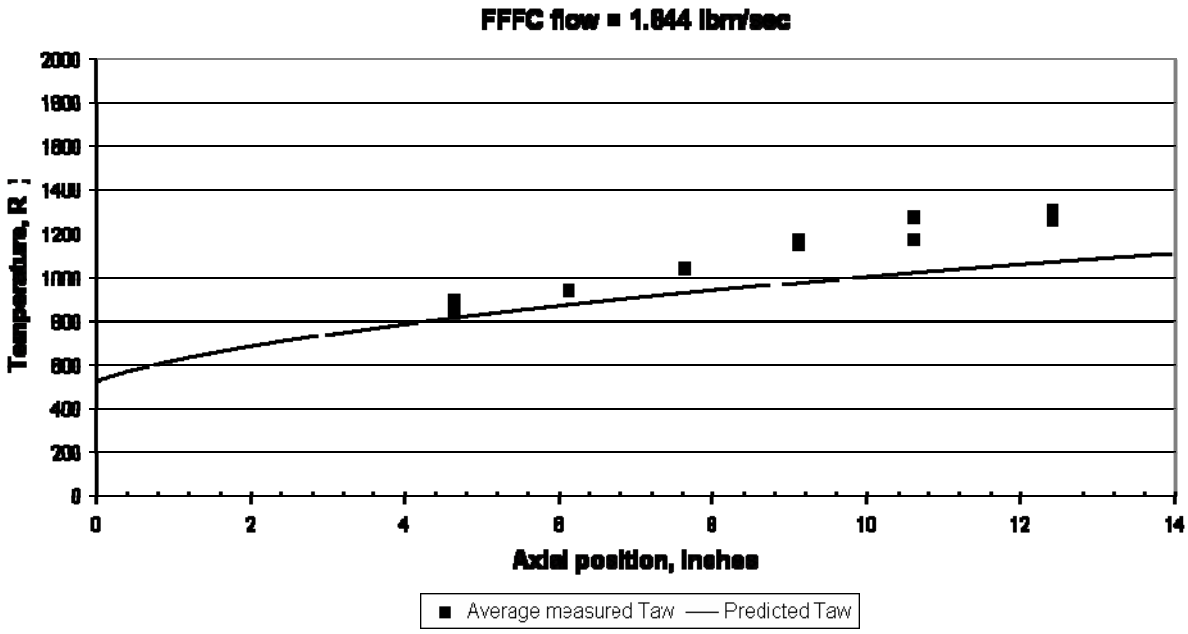

Figure 7 Predicted and averaged experimental results for 11905-162107.

D. 11905 131613 test results

Figure 8 presents the measured, average hot wall temperature as compared to the predicted hot wall temperature for test 11905-131613. The cooling model consistently underpredicted the wall temperature as with Test 11705-231534 with differences ranging from -30% to -47%. The reason for this large discrepancy is discussed in Section IV. Table 3 shows a film cooling mass flow of 3.617 lb_m/s for this test.

The heat flux data from the thermocouples remain similar to previous tests, and the magnitudes of the measured heat fluxes compare similarly to the applied heat fluxes with the same trends as before.[16]

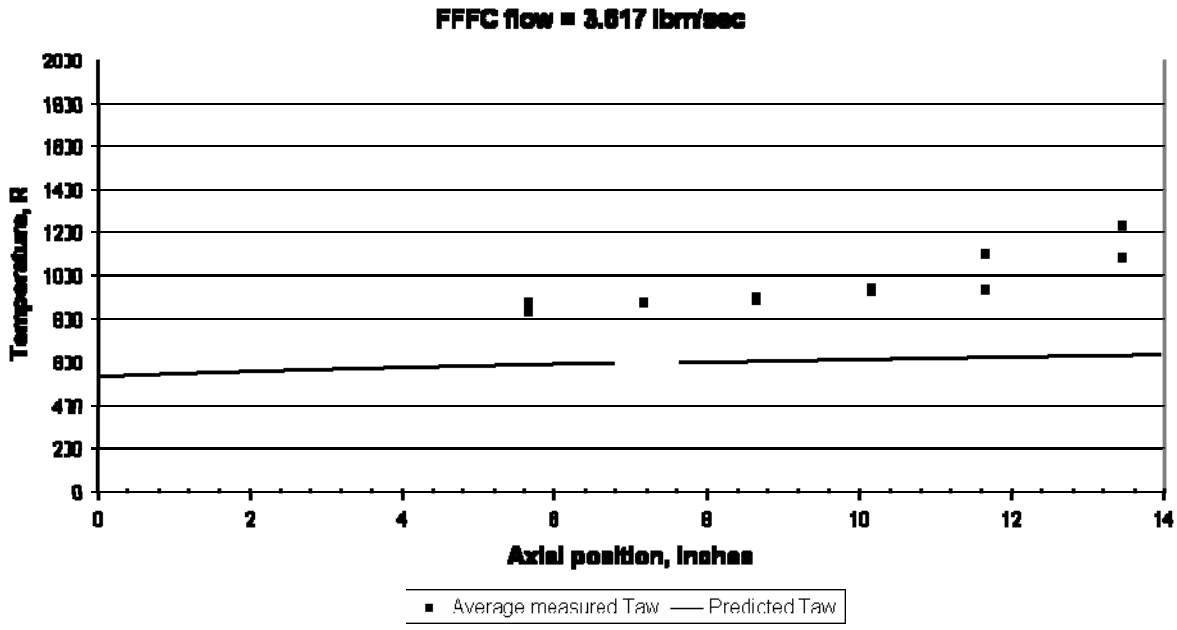

Figure 8 Predicted and average measured results for test 11905-131613.

E. 112205 180505

Figure 9 presents the measured, average hot wall temperature as compared to the predicted hot wall temperature for test 112205-180505. This test had a film cooling flow rate of 1.643 lbm/sec which was similar to test 11905 171710. The differences ranged from approximately -15% to 10%. Data from Reference 16 indicated that there was a large circumferential variation in the measured wall temperature around x = 10.5 inches. TBAR5, the second thermocouple around x = 7-in, had its data dropped for the heat flux analyses. TBAR5 had not been dropped in the previous two experiments, and it showed significant variation with TBAR6, its circumferential counterpart. This suggests that the large circumferential variation in temperature at x = 7 was due to a sensor problem rather than a real physical phenomenon.

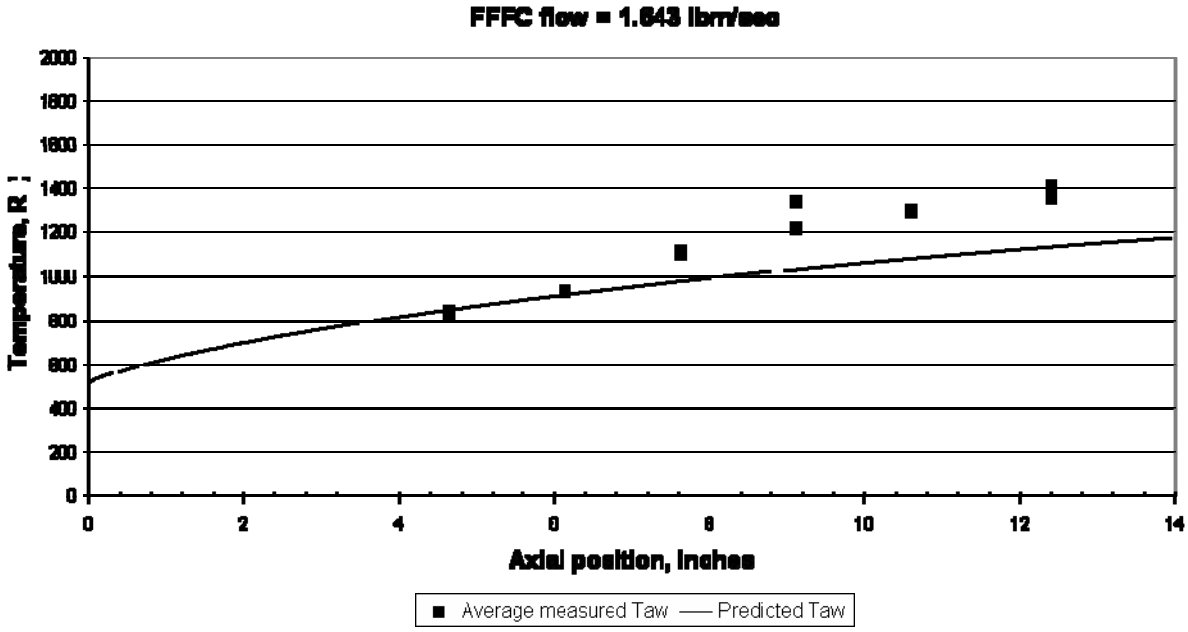

Figure 9 Predicted and average measured results for test 112205-180505.

F. 12606 192840

Figure 10 presents the measured, average hot wall temperature as compared to the predicted hot wall temperature for test 12606-192840. The final test examined a very low FFFC flow rate of 0.88 lb_m/s. Differences between measurement and prediction ranged from about -5% to about 32%. This was the only test where the liquid film model predicted temperatures high enough to meaningfully test the entrainment model, explored in more detail in Reference 16. The liquid film model predicted temperatures that slightly exceeded 1510 ^oR which was the temperature where the onset of significant endothermic cracking reactions would appear.

Although not immediately apparent, Figure 10 has two plots which compare the predicted wall temperature without the endothermic effect and with the effect. The two lines are superimposed, possibly implying that the cracking reactions were insignificant. However, since the film temperature did not reach ~ 1510 ^oR until very near the end of the test section, perhaps there was not enough time to see a significant effect of the cracking reactions.

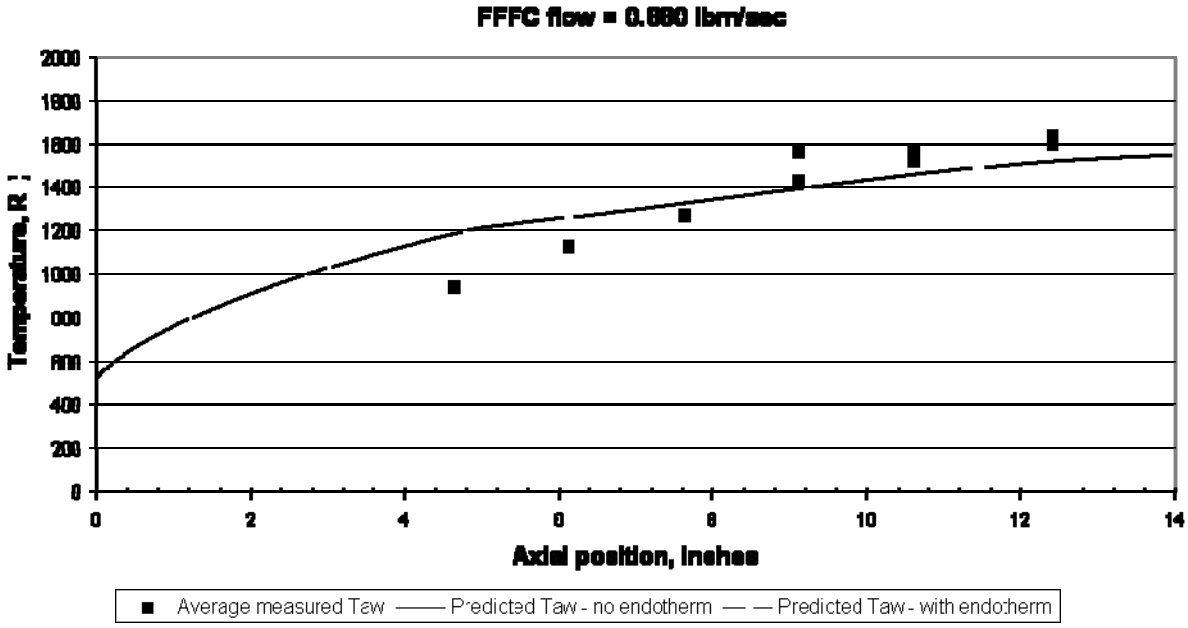

Figure 10 Predicted and average measured results for test 12606-192840.

IV. Conclusions

A supercritical liquid film cooling model was developed based on modifications to techniques presented in the literature. The model provides a reasonable first-order analysis of film cooling analysis for an RP-1/GOX LRE using RP-1 coolant at sub-cooled liquid conditions. The model was compared to test data from the constant area section of the combustion chamber.

Coaxial thermocouples were used to measure gas-side wall temperatures and derive gas-side wall heat fluxes. In general, the derived heat fluxes increased slightly down the barrel, a trend that was present in all tests. The derived gas-side wall heat fluxes were sometimes as much as 50% of the total applied heat flux from the core gases to the coolant, implying that the adiabatic wall assumption was not justified. This in turn implies the test had not reached steady state conditions before the hot fire portion of the test was terminated.

The liquid film cooling model consistently predicted the inside wall temperature with less than 33% error in four out of five cases for a constant cross-sectional area chamber. The error could vary substantially with axial position for the same test. The sigmoid shape of the liquid film prediction caused its temperature predictions to rise faster than the experimental temperature measurements near the injector, but slower than experimental measurements as

one moves downstream. This sigmoid shape was partly due to the use of a flat plate correlation for computing the gas side heat transfer coefficient, as these correlations universally predict a large heat transfer coefficient near the leading edge that decreases rapidly at first, and then more slowly as one moves downstream. In addition, the assumption of constant liquid film thickness until the supercritical transition enhanced this shape by forcing the liquid surface to accelerate as its density decreased due to heating. This reduced the velocity differential between the core gases and the liquid surface as one moves downstream, which in turn forced the heat transfer coefficient to be lower than it would have been had the surface film velocity remained roughly constant. This effect was especially pronounced in test 11905-131613 which had a very high FFFC flow rate. Therefore, it is suggested that a better assumption or a method to compute the film thickness be used in the future when studying liquid film cooling under supercritical conditions. Grissom's method of computing the film thickness is derived from considering mass transfer from the liquid surface to the core gases by evaporation under sub-critical conditions, a possibility that does not exist under supercritical conditions and thus can not be implemented here. Also, a different heat transfer correlation may improve the predictive model – perhaps a turbulent pipe flow correlation would be more appropriate and yield a better correlation between the predictive model and experimental measurements.

The turbulence intensity has a moderately strong effect on the predicted heat flux for the liquid film model; therefore, additional research should be performed to assess the actual turbulence level of the core gases. This would presumably strengthen the turbulence model assumption especially with regard to estimating the turbulence intensity.

The radiation model ignored the emissivity of carbon monoxide and other species which were likely present in non-negligible mole fractions. Unfortunately, much additional gas radiation research is needed before truly reliable total gas emissivity predictions are possible. Since the core gases are extremely hot, radiation can not be neglected even if total emissivity values are relatively low. Therefore, better radiation models would be profitable.

Only one test ran "hot enough" to test the endothermic cracking model. No difference was seen between the prediction without the endothermic model and the prediction with the endothermic model due to the small coolant temperature rise above 1510 ^{o}R before the end of the barrel. This result has to be accepted cautiously, since additional data to corroborate or contradict these findings are not presented.

Acknowledgments

The authors thank C.W. Johnson of Sierra Engineering Incorporated and Yen Yu of Purdue University for offering their insights into the film cooling problem, and Paul (Kevin) Tucker of NASA Marshall Space Flight Center who was the technical point of contact for the funding agency during the test program funded under contract NNM05AA67C. In addition, Dr. Chris Sturgis is acknowledged as the technical point of contact for the Air Force for contract F04611-00-C-0009 under which Sierra Engineering Inc. designed and fabricated this test hardware.

References

1. Crocco, L., "An Approximate Theory of Porous, Sweat, or Film Cooling With Reactive Fluids," *ARS Journal*, November-December 1952, pp. 331-338.

2. Dorrance, W.H. and Dore, F.J., "The Effect of Mass Transfer on the Compressible Turbulent Boundary-Layer Skin Friction and Heat Transfer," *Journal of the Aeronautical Sciences*, June 1954, pp. 404-410.

3. Hatch, J.E. and Papell, S.S., "Use of a Theoretical Flow Model to Correlate Data for Film Cooling or Heating an Adiabatic Wall by Tangential Injection of Gases of Different Fluid Properties," NASA TN D-130, 1959.

4. Seban, R.A., "Heat Transfer and Effectiveness for a Turbulent Boundary Layer with Tangential Fluid Injection," *Journal of Heat Transfer*, November, 1960, pp. 303-312.

5. Seban, R.A. and Back, L.H., "Velocity and Temperature Profiles in Turbulent Boundary Layers with Tangential Injection," *Journal of Heat Transfer*, February, 1962, pp. 45-54.

6. Stollery, J.L., El-Ehwany, A. A. M., "A Note on the Use of A Boundary-Layer Model for Correlating Film-Cooling Data," *Int, J. Heat and Mass Transfer*, Vol. 8, 1965, pp. 55-65.

7. Spalding, D.B., "Prediction of Adiabatic Wall Temperatures in Film-Cooling Systems," *AIAA Journal*, Vol. 3, No. 5, pp. 965-967.

8. Warner, C.F., and Emmons, D.L., "Effects of Selected Gas Stream Parameters and Coolant Properties on Liquid Film Cooling," *Journal of Heat Transfer*, May, 1964, pp. 271-278.

9. Hansmann, T. and Wilhelmi, H., "An Experimental Investigation of the Film-Cooling Process at High Temperatures and Velocities," *AIAA-93-5062*, 1993, pp. 1-8.

10. Kinney, G.R., Abramson, A.E., and Sloop, J.L., "Internal-Liquid-Film-Cooling Experiments with Air-Stream Temperatures to 2000°F in 2- and 4-Inch-Diameter Horizontal Tubes," NACA Report 1087, Lewis Flight Propulsion Laboratory, Cleveland, OH, 1952.

11. Knuth, E.L., "The Mechanics of Film Cooling," Ph.D. dissertation, California Institute of Technology, Pasadena, CA, 1954.

[12.] Gater, R.A. and L'Ecuyer, M.R., "A Fundamental Investigation of the Phenomena that Characterize Liquid-Film Cooling," Technical Memorandum, Contract Nonr 1100(21) and NASA Grant NsG 592, Jet Propulsion Laboratory, Purdue University, West Lafayette, IN, 1969.

[13.] Stechman, R.C., "Film Cooling of Small Rocket Engines," M.S. Thesis, San Fernando Valley State College, Mechanical Engineering Department, Northridge, CA, 1968.

[14.] Grissom, W.M., "Liquid Film Cooling in Rocket Engines," Arnold Engineering Development Center, AEDC-TR-91-1, Arnold AFB, TN, 1991.

[15.] Yu, Y.C., "Liquid Film Cooling in a Model Combustor Using Swirl Injection," M.S. Thesis, School of Aeronautics and Astronautics, Purdue University, West Lafayette, IN, 2005.

[16.] Haberlen, P.A., "Supercritical Fuel Film Cooling in a RP-1/Gox Staged Combustion Rocket," M.S. Thesis, School of Aeronautics and Astronautics, Purdue University, West Lafayette, IN, 2006.

[17.] Rousar, D.C. and Ewen, R.L., "Hydrogen Film Cooling Investigation," ALRC Final Report, Contract NAS 3-15844, NASA CR-121235, August, 1973.

[18.] Rousar, D.C. and Ewen, R.L., "Combustion Effects on Film Cooling," NASA CR-135052, Contract No. NAS 3-17813, Sacramento, CA, 1976.

[19.] Long, M.R., Bazarov, V.G., and Anderson, W.E., "Main Chamber Injectors for Advanced Hydrocarbon Booster Engines," *AIAA Paper 2003-4599*.

[20.] Edwards, T., "Kerosene fuels for Aerospace Propulsion – Composition and Properties," AIAA 2002-3874, 38th AIAA/ASME/SAE/ASEE Joint Propulsion Conference and Exhibit, Indianapolis, IN, 2002.

[21.] Sheu, J.-C., Zhou, N., and Krishnan, A., "Thermal Cracking of Norpar-13 Fuel under near-critical and Supercritical Conditions," AIAA 98-3758, 34th AIAA/ASME/SAE/ASEE Joint Propulsion Conference and Exhibit, Cleveland, OH, 1998.

[22.] Yu, J. and Eser., "Thermal Decomposition of C10-C14 Normal Alkanes in Near-Critical and Supercritical Regions: Product Distributions and Reaction Mechanism," *Ind. Eng. Chem. Res*., Vol. 36, 1997, pp. 574-584.

[23.] Yu, J. and Eser., "Kinetics of Supercritical-Phase Thermal Decomposition of C10-C14 Normal Alkanes and Their Mixtures," *Ind. Eng. Chem. Res*., Vol. 36, 1997, pp. 585-591.

[24.] Edwards, T. and Zabarnick, S., "Supercritical Fuel Mechanisms," *Ind. Eng. Chem. Res*., Vol. 32, 1993, pp. 3117-3122.

[25.] Huang, H., Spadaccini, L.J., Sobel, D.R., "Fuel-Cooled Thermal Management for Advanced Aeroengines," *Transactions of the ASME*; *Journal of Engineering for Gas Turbines and Power*, Vol. 126, 2004, pp. 284-293.

[26.] Churchill, S.W. and Usagi, R., "A General Expression for the Correlation of Rates of Transfer and other Phenomena," *AIChE Journal*, Vol. 18, No. 6, 1972, pp. 1121-1128.

[27.] Barbin, A.R. and Jones, J.B., "Turbulent Flow in the Inlet Region of a Smooth Pipe," *Trans. ASME – Journal of Basic Engineering*, March 1963, pp. 29.

[28.] Pletcher, R.H., "Progress in Turbulent Forced Convection," *Trans. ASME; Journal of Heat Transfer*, Vol. 110, 1988, pp. 1129.

[29.] Hersch, M., *ARS Journal*, Vol. 31, 1961, pp. 39.

[30.] Talmor, E., *A.I.Ch.E. Journal*, Vol. 12, 1966, pp. 1092.

[31.] Siegel, R. and Howell, J.R., *Thermal Radiation Heat Transfer*, 2nd ed., Hemisphere, Washington, 1981, Sections 17.5 – 17.6.

[32.] Ziebland, H. and Parkinson, R.C., "Heat Transfer in Rocket Engines," *AGARD-AG-148-71*, 1971, Chapter 6.

[33.] Patankar, S.V., *Numerical Heat Transfer and Fluid Flow*, Hemisphere Publishing, Washington, 1980.

[34.] Hoffman, J.D., *Numerical Methods for Engineers and Scientists*, 2nd ed., Marcel Dekker, New York, 2001.

[35.] Cook, W.J., "Determination of Heat-Transfer Rates from Transient Surface Temperature Measurements," *AIAA Journal*, Vol. 8, No. 7, 1970, pp. 1366-1368.

[36.] Kidd, C.T., "Coaxial Surface Thermocouples – Analytical and Experimental Considerations for Aerothermal Heat-flux Measurement Applications," *AIAA Journal*, 0227-7576, 1990, pp. 203-211.

[37.] Cook, W.J., "Reduction of Data from Thin-Film Heat-Transfer Gages: A Concise Numerical Technique," *AIAA Journal*, Vol. 4, No. 3, 1996, pp. 561-562.

[38.] Bezuidenhout, J.J., Schetz, J.A., and Walker, D.G., "Heat Flux Determination Using Surface and Backface Temperature Histories and Inverse Methods," *AIAA Journal 2001-3530*, 2001, pp. 1-11.

[39.] Childs, P.R.N., Greenwood, J.R., and Long, C.A., "Heat flux measurement techniques," *Proc. Instn. Mech. Engrs*, Vol. 213, Part C, pp 655-677.

[40.] "Bulletin 500," Medtherm Corporation, Huntsville, AL, 2002.

[41.] "Installation Suggestions for 0.061" Dia Insulated Junction Coaxial Thermocouples," Medtherm Corporation, Hunstville, AL.

[42.] Engineering drawing number 11354, "TCS-061-M-L-CR-YYY-11354 Coaxial surface thermocouple", Medtherm Corporation, Huntsville, AL, 2001.

[43.] Kuo, C.H. and Kulkarni, A.K., "Analysis of heat flux measurement by circular foil gages in a mixed convection/radiation environment," *Journal of Heat Transfer*, Vol. 113, 1991, pp. 1037-1040.

[44.] Incropera, F.P. and DeWitt, D.P., *Fundamentals of Heat and Mass Transfer*, 4th ed., John Wiley & Sons, New York, 1996.

[45.] Hoskins Manufacturing Co., Hoskins Chromel (P)/Alumel Thermocouple Alloys, Catalog M61 C-A, 12/68.

[46.] Sundqvist., "Thermal Diffusivity and Thermal Conductivity of Chromel, Alumel, and Constantan in the Range 100-450K," *J. Appl. Phys*., Vol. 72, No. 2, 1992, pp. 539.

[47.] Kendall, D.N. and Dixon, W.P., "Heat Transfer Measurements in a Hot Shot Wind Tunnel," McDonnell Aircraft Corporation, *IEEE Aerospace Systems Conference*, Seattle, WA, 11-15 July, 1966.

[48.] Turns, S.R., *An Introduction to Combustion,* 2nd ed., McGraw-Hill, Boston, 2000, pp. 343-346 and pp. 458-459.

[49.] Schoenman, L., Block, P., "Application of Laminar Boundary Layer Heat Transfer Theory to low Thrust Rocket Nozzle," AIAA-67-447, 3rd Propulsion Joing Specialist Conference, Washington, D. C., July 1967.

[50.] Ewen, Evensen, "Liquid Rocket Engine Self-Cooled Combustion Chambers," NASA-SP-8126, Sep. 1977.